Macromolecules
Article
pubs.acs.org/Macromolecules

Copper-Catalyzed Polycoupling of Diynes, Primary Amines, and Aldehydes: A New One-Pot Multicomponent Polymerization Tool to Functional Polymers

Yajing Liu,[†,‡] Meng Gao,[†,‡] Jacky W. Y. Lam,*[,†,‡] Rongrong Hu,[†,‡] and Ben Zhong Tang*[,†,‡,§]

[†]HKUST-Shenzhen Research Institute, No. 9 Yuexing first RD, South Area, Hi-tech Park, Nanshan Shenzhen 518057, China

[‡]Department of Chemistry, Division of Life Science, State Key Laboratory of Molecular Neuroscience, Institute for Advanced Study, Institute of Molecular Functional Materials, Division of Biomedical Engineering, The Hong Kong University of Science and Technology, Clear Water Bay, Kowloon Hong Kong, China

[§]Guangdong Innovative Research Team, SCUT-HKUST Joint Research Laboratory, State Key Laboratory of Luminescent Materials and Devices, South China University of Technology, Guangzhou 510640, China

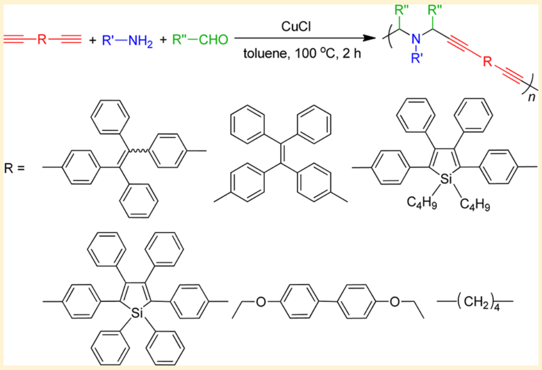

ABSTRACT: Development of new methodology for the preparation of functional polymers with practical applications is a fundamental important research area in macromolecular science. In this paper, a new polymerization route for the synthesis of functional polymers is developed. The three-component polycoupling reactions of diynes [HC≡C−R−C≡CH, R = $(C_6H_5)_2C{=}C(C_6H_5)_2$, $(C_6H_5)_4SiC_4(C_4H_9)_2$, $(C_6H_5)_4SiC_4(C_6H_5)_2$, $C_{12}H_8(OCH_2)_2$, $(CH_2)_4$], primary amines, and aldehydes are catalyzed by copper(I) chloride in toluene at 100 °C for 2 h, affording soluble and regular poly(dipropargyl amine)s (PDAs) with high molecular weights (M_w up to 43 800) in high yields (up to 89%). The polymerization reaction is insensitive to moisture. All the PDAs are thermally stable and film forming. Their thin films show good optical transparency and high refractive indices (RI = 1.8322−1.7458) with low optical dispersions (D down to 0.0117). The tetraphenylethene or silole-containing PDAs exhibit a phenomenon of aggregation-induced emission. The PDAs are photosensitive and cross-link upon UV irradiation, generating negative photoresist fluorescent patterns. The polymer aggregates can function as sensitive fluorescent chemosensors for detecting explosives, such as picric acid, 2,4-dinitrotoluene, and 4-nitrobenzoyl chloride, with large quenching constants of up to 2.7×10^5 L/mol.

■ INTRODUCTION

The development of a novel polymerization route to functional polymer with unique properties is a fundamental important area in macromolecule science. Compared with numerous existing polymers with single-bond structures, those constructed from acetylenic monomers tend to be more electronically active. The conjugated olefin scaffolds endow the polymers with unique electronic, mesomorphic, photonic, and biological properties. However, most of these polymers are obtained from single monomer or polymerization between two components. Multicomponent polymerization tools, however, are scarcely reported in the past decade.[1]

Multicomponent reactions (MCRs) have attracted much attention from organic chemists because of their various advantages.[2] MCRs proceed in chemo- and regioselective fashion with high atom economy and diminution of waste production due to the reduced synthetic and isolation steps, thus allowing the preparation of complex compounds from simple precursors. In 2002, Li and co-workers discovered the A^3-coupling reactions of alkynes, aldehydes, and amines, and since then they have made remarkable progress in this area.[3] Konakahara,[4] Wang,[5] Damavandi,[6] and Cai[7] augmented the reaction scope and enriched the catalyst system during the past decade. In 2012, Li reported the copper-catalyzed A^3-coupling reaction of alkyne, amino acid, and aldehyde under ambient aqueous conditions, generating dipropargylated products in high yields.[8]

For many years, our group has been working on the construction of functional macromolecules from monoynes, diynes, and triynes by means of one or two-component metathesis polymerization, polycoupling, polycyclotrimerization, and "click" reaction.[9] Recently, we succeeded in the generation of soluble polymers with well-defined structures by indium-catalyzed three-component polycoupling of diyne, dialdehyde, and secondary amine (Scheme 1).[10] The polymers have been found to exhibit a variety of unique properties such as strong emission in the aggregated state, high refractive indices, and precursors to nanostructured magnetic ceramics.[11]

Received: July 18, 2014
Published: July 23, 2014

Scheme 1. Indium-Catalyzed Polycoupling of Diyne, Amine, and Dialdehyde

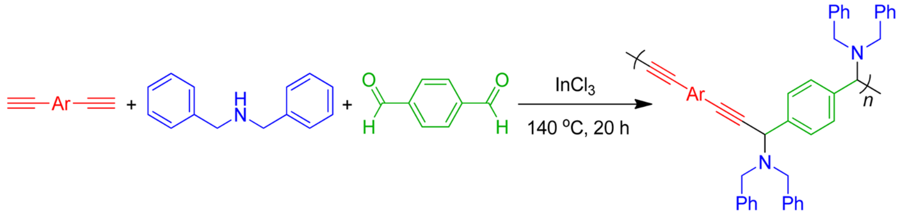

Scheme 2. Copper-Catalyzed Polycoupling of Diynes, Amines, and Aldehydes

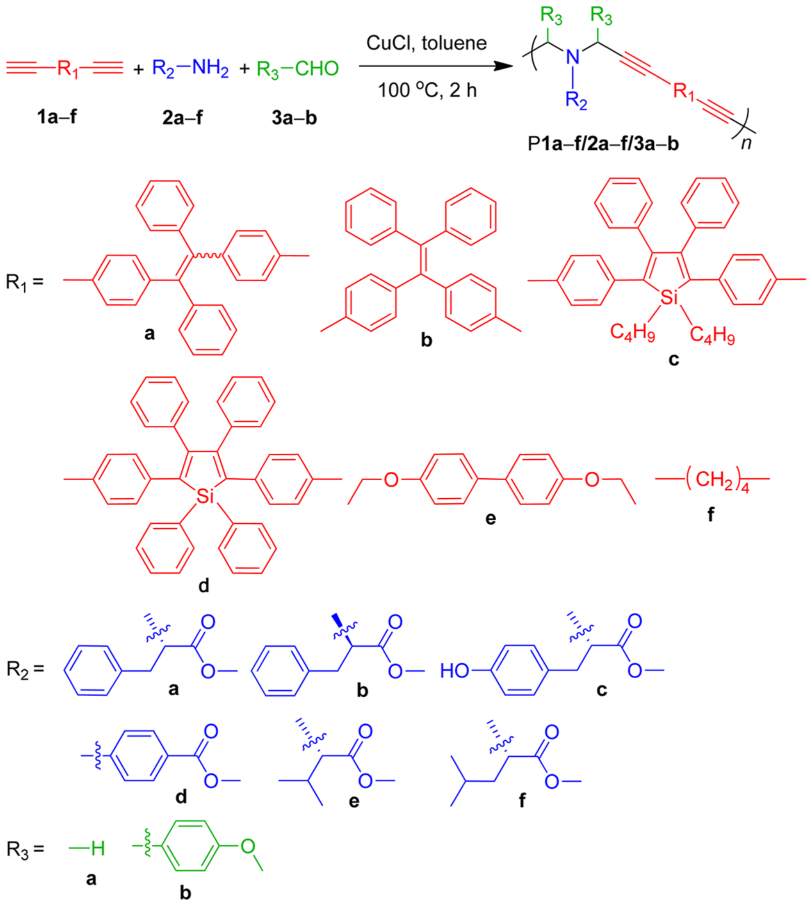

The indium-catalyzed three-component polymerization, however, has some drawbacks: the catalyst ($InCl_3$) is expensive, and the polymerization only proceeds smoothly at a high temperature of 140 °C for a long reaction time of 20 h. Therefore, it would be nice if a similar polymerization pathway can be developed, which can perform under milder reaction conditions without the requirement of costly catalyst or additive.

In this paper, we show that the polycoupling reactions of diynes, primary amines, and aldehydes can be carried out at a lower temperature of 100 °C for only 2 h in the presence of a less expensive catalyst of copper(I) chloride, furnishing soluble poly(dipropargylamine)s (PDAs) with high molecular weights in high yields (Scheme 2). The polymerization reaction is insensitive to moisture. The obtained PDAs are thermally stable. Their thin films show high refractive indices and cross-link upon UV irradiation, generating negative photoresist patterns. The PDAs carrying tetraphenylethene (TPE) and silole chromophores exhibit a phenomenon of aggregation-induced emission (AIE), and their aggregates can function as sensitive fluorescent chemosensors for explosive detection. All these attributes make them to find potential high technological applications.

■ EXPERIMENTAL SECTION

Materials and Instrumentation. Tetrahydrofuran (THF) was distilled from sodium benzophenone ketyl under nitrogen immediately before use. All the primary amines, aldehydes, and other reagents were purchased from Aldrich and used as received without further purification. Monomers, named 1,2-bis(4-ethynylphenyl)-1,2-diphenylethene (**1a**),[12a] 2,5-bis(4-ethynylphenyl)-3,4-diphenyl-1,1-dibutylsilole (**1c**),[12c] 2,5-bis(4-ethynylphenyl)-1,1,3,4-tetraphenylsilole (**1d**),[12c] and 1-(4-ethynylphenyl)-1,2,2-triphenylethene (**9**),[12d] were prepared according to the literature methods. 4,4′-Bis(2-ethynyloxy)-biphenyl (**1e**) was prepared by nucleophilic substitution of 4,4′-biphenol with propargyl bromide.[12b] Weight-average molecular weights (M_w) and polydispersities (M_w/M_n) of the polymers were estimated on a Waters gel permeation chromatography (GPC) system using THF as eluent. Details about the experimental setup can be found in our previous publication.[10]

Scheme 3. Synthetic Route to Tetraphenylethene-Containing Diyne

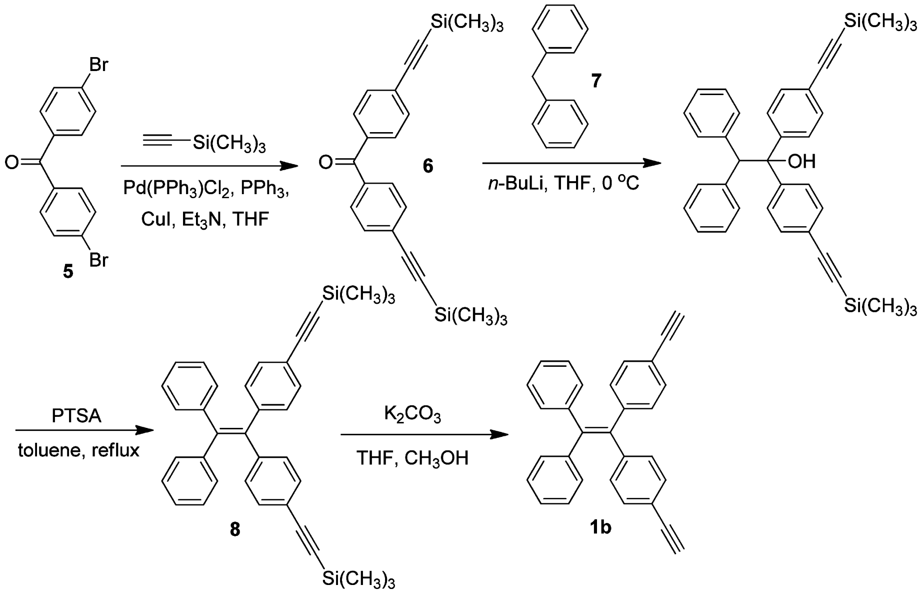

IR spectra were recorded on a PerkinElmer 16 PC FTIR spectrophotometer. ^{1}H and ^{13}C NMR spectra were measured on a Bruker AV 400 spectrometer in deuterated chloroform using tetramethylsilane (TMS; δ = 0) as internal reference. UV spectra were measured on a Milton Ray Spectronic 3000 Array spectrophotometer. Photoluminescence (PL) spectra were recorded on a PerkinElmer LS 55 spectrophotometer. Thermogravimetric analysis (TGA) was carried on a TA TGA Q5000 under nitrogen at a heating rate of 10 °C/min. Particle sizes of the polymer aggregates were measured on a Brookhaven Zeta potential analyzer. Refractive indices were determined on a J.A. Woollam variable angle ellipsometry system with a wavelength tunability from 300 to 1000 nm.

Monomer Synthesis. Monomer **1b** was synthesized according to the synthetic route shown in Scheme 3. Detailed procedures are shown below.

Synthesis of 4,4′-Bis(2-trimethylsilylethynyl)benzophenone (6). Into a 500 mL two-necked round-bottom flask were added 4,4′-dibromobenzophenone (**5**, 10 g, 29.4 mmol), $Pd(PPh_3)_2Cl_2$ (619 mg, 0.88 mmol), CuI (223 mg, 1.17 mmol), PPh_3 (154 mg, 0.59 mmol), THF (150 mL), and triethylamine (50 mL) under a nitrogen atmosphere. After all the solids were completely dissolved, (trimethylsilyl)acetylene (16.6 mL, 117.6 mmol) was injected into the flask. After stirring at 70 °C overnight, the reaction was quenched with the addition of an aqueous solution of ammonium chloride. The reaction mixture was extracted with dichloromethane (3 × 50 mL). The organic layers were combined and dried over anhydrous magnesium sulfate. The solvent was evaporated, and the resulting crude product was purified on a silica gel column chromatography using hexane as eluent. White solid; yield 81.6%. ^{1}H NMR (400 MHz, $CDCl_3$), δ (TMS, ppm): 7.72 (d, 4H), 7.57 (d, 4H), 0.27 (18H).

1,1-Bis[4-(2-trimethylsilylethynyl)phenyl]-2,2-diphenylethene (8). To a solution of diphenylmethane (**7**, 3.23 g, 19.2 mmol) in THF (20 mL) was added dropwise 2 M solution of *n*-butyllithium in hexane (7.68 mL, 15.36 mmol) at 0 °C under nitrogen. After stirring for 30 min, a solution of **6** (2.1 g, 12.8 mmol) in THF was added into the solution. After warming to room temperature and stirring overnight, the reaction was quenched with the addition of an aqueous solution of ammonium chloride. The organic layer was extracted with dichloromethane (3 × 50 mL) and saturated aqueous solution of sodium chloride. The combined organic layers were dried over anhydrous magnesium sulfate. After filtration, the solvent was evaporated and the resulting crude alcohol (containing excess diphenylmethane) was dissolved in 80 mL of toluene in a 250 mL two-necked round-bottom flask equipped with a condenser. A catalytic amount of *p*-toluenesulfonic acid was added, and the mixture was refluxed for 4 h. After cooling to room temperature, the organic layer was washed with 10% aqueous $NaHCO_3$ solution (3 × 30 mL) and dried over anhydrous magnesium sulfate. After filtration and solvent evaporation, the crude product was purified on a silica gel column chromatography using hexane/ethyl acetate (10:1 v/v) as eluent. Yellow solid; yield 71.5%. ^{1}H NMR (400 MHz, $CDCl_3$), δ (TMS, ppm): 7.20 (m, 4H), 7.09 (m, 8H), 6.97 (m, 6H), 0.22 (s, 16H).

1,1-Bis(4-ethynylphenyl)-2,2-diphenylethene (1b). Into a 250 mL two-necked round-bottom flask was added **8** (2.1 g, 12.8 mmol), excess potassium carbonate, tetrahydrofuran (50 mL), and methanol (50 mL). After stirring for 3 h, the reaction was quenched with the addition of 10% aqueous solution of hydrochloric acid. The organic layer was extracted with dichloromethane (3 × 50 mL), and the combined organic layers were dried over anhydrous magnesium sulfate. After filtration and evaporation, the crude product was purified on a silica gel column chromatography using hexane as eluent. White solid; yield 70.8%. ^{1}H NMR (400 MHz, $CDCl_3$), δ (TMS, ppm): 7.24–7.22 (m, 4H), 7.12–7.11 (m, 6H), 7.01–6.95 (m, 8H), 3.04 (s, 2H). ^{13}C NMR (100 MHz, $CDCl_3$), δ (TMS, ppm): 143.02, 142.59, 139.23, 131.28, 127.85, 126.89, 120.07, 83.67. HRMS (MALDI-TOF): *m/z* 380.1525 [M^+, calcd 380.1565].

Polymer Synthesis. All the polymerization reactions were carried out under nitrogen using the standard Schlenk technique. A typical experimental procedure for the polymerization of **1a** with **2a** and **3a** is given below as an example.

Into a 10 mL Schlenk tube equipped with a magnetic stirrer were placed **1a** (0.1 mmol), **2a** (0.1 mmol), and **3a** (0.3 mmol, 38 wt % formaldehyde solution), CuCl (0.5 equiv to **1a**), and $NaHCO_3$ (0.1 mmol) in 0.1 mL of distilled toluene. The reaction mixture was stirred under nitrogen in an oil bath at 100 °C for 2 h. Afterward, the polymerization reaction was stopped by pouring the reaction mixture into 150 mL of hexane via a cotton filter to remove any, if possible, insoluble substances and the Cu catalyst. The precipitates were washed with hexane and dried in vacuum overnight at 40 °C to a constant weight.

Characterization Data for P1a/2a/3a. Yellow solid; yield 82.0% (Table 6, entry 1). M_w 29 200; M_w/M_n 4.6 (GPC, polystyrene calibration). IR (KBr), υ (cm^{-1}): 3031, 2951, 1731, 1602, 1498, 1442. ^{1}H NMR (400 MHz, $CDCl_3$), δ (TMS, ppm): 7.24, 7.19, 7.17, 7.10, 6.99, 6.94, 3.88, 3.48, 3.10. ^{13}C NMR (100 MHz, $CDCl_3$), δ (TMS, ppm): 172.16, 144.54, 143.39, 142.89, 141.21, 140.98, 140.75, 140.54, 137.46, 131.73, 131.17, 129.09, 128.27, 127.79, 126.72, 126.46, 120.99, 119.72, 85.01, 81.84, 65.76, 51.45, 40.97, 36.39, 36.26, 31.34.

P1b/2a/3a. Greenish-yellow solid; yield 59.2% (Table 6, entry 2). M_w 16 700; M_w/M_n 2.0 (GPC, polystyrene calibration). IR (film), ν (cm^{-1}): 2926, 2857, 1735, 1663, 1600, 1496, 1451. ^1H NMR (400 MHz, $CDCl_3$), δ (TMS, ppm): 7.24, 7.21, 7.18, 7.17, 7.15, 7.10, 7.00, 6.99, 6.94, 6.92, 3.88, 3.48, 3.10. ^{13}C NMR (100 MHz, $CDCl_3$), δ (TMS, ppm): 143.40, 143.18, 137.55, 131.24, 131.14, 129.19, 129.02, 128.37, 128.21, 127.80, 126.79, 126.55, 125.28, 121.00, 85.13, 51.56, 41.06, 30.91.

P1c/2a/3a. Orange solid; yield 50.7% (Table 6, entry 3). M_w 15 700; M_w/M_n 2.2 (GPC, polystyrene calibration). IR (KBr), ν (cm^{-1}): 3025, 2956, 2921, 2855, 1734, 1656, 1597, 1437. ^1H NMR (400 MHz, $CDCl_3$), δ (TMS, ppm): 7.19, 7.00, 6.82, 6.77, 3.89, 3.49, 3.12, 2.36, 1.32, 0.99, 0.81. ^{13}C NMR (100 MHz, $CDCl_3$), δ (TMS, ppm): 155.79, 142.94, 142.43, 140.47, 138.54, 131.35, 129.22, 129.00, 128.70, 128.34, 127.47, 126.35, 125.27, 119.82, 26.04, 25.64, 21.43, 11.62.

P1d/2a/3a. Yellow solid; yield 52.7% (Table 6, entry 4). M_w 2700; M_w/M_n 2.0 (GPC, polystyrene calibration). IR (film), ν (cm^{-1}): 2958, 2918, 2850, 1735, 1666, 1597, 1431. ^1H NMR (400 MHz, $CDCl_3$), δ (TMS, ppm): 7.64, 7.38, 7.10, 7.04, 6.98, 6.86, 6.84, 6.56, 3.52, 301, 2.81. The ^{13}C NMR data were not obtained due to the low solubility of the obtained polymer.

P1e/2a/3a. Yellow solid; yield 14.6% (Table 6, entry 5). M_w 2100; M_w/M_n 1.8 (GPC, polystyrene calibration). IR (film), ν (cm^{-1}): 2924, 1723, 1604, 1495, 1446. ^1H NMR (400 MHz, $CDCl_3$), δ (TMS, ppm): 7.46, 7.44, 7.43, 7.31, 7.19, 7.10, 7.02, 7.00, 6.99, 4.75, 4.73, 4.72, 3.67, 3.50, 2.98, 2.55. ^{13}C NMR (100 MHz, $CDCl_3$), δ (TMS, ppm): 171.03, 129.05, 128.28, 127.67, 115.08, 60.28, 55.78, 30.80, 29.60, 20.92, 14.08.

P1f/2a/3a. Red oil; yield 12.7% (Table 6, entry 6). M_w 1500; M_w/M_n 1.6 (GPC, polystyrene calibration). ^1H NMR (400 MHz, $CDCl_3$), δ (TMS, ppm): 7.20, 7.17, 3.75−3.72, 3.53, 3.02, 2.23, 1.62. The ^{13}C NMR data were not obtained due to the low solubility of the obtained polymer.

P1a/2b/3a. Brown solid; yield 56.7% (Table 6, entry 7). M_w 11 800; M_w/M_n 2.2 (GPC, polystyrene calibration). IR (KBr), ν (cm^{-1}): 3031, 2951, 1731, 1602, 1498, 1442. ^1H NMR (400 MHz, $CDCl_3$), δ (TMS, ppm): 7.24, 7.19, 7.17, 7.10, 6.99, 6.94, 3.88, 3.48, 3.10. ^{13}C NMR (100 MHz, $CDCl_3$), δ (TMS, ppm): 172.16, 144.54, 143.39, 142.89, 141.21, 140.98, 140.75, 140.54, 137.46, 131.73, 131.17, 129.09, 128.27, 127.79, 126.72, 126.46, 120.99, 119.72, 85.01, 81.84, 65.76, 51.45, 40.97, 36.39, 36.26, 31.34.

P1a/2c/3a. Brown solid; yield 57.1% (Table 6, entry 8). IR (KBr), ν (cm^{-1}): 2923, 1735, 1656, 1600, 1493, 1438, 1211, 1166, 1105, 1016. The GPC and NMR data were not obtained as the obtained polymer was insoluble.

P1a/2d/3a. Orange solid; yield 7.2% (Table 6, entry 9). M_w 4100; M_w/M_n 1.7 (GPC, polystyrene calibration). IR (film), ν (cm^{-1}): 2957, 1715, 1604, 1512, 1437. ^1H NMR (400 MHz, $CDCl_3$), δ (TMS, ppm): 7.95, 7.15, 7.07, 6.99, 6.94, 6.89, 6.87, 4.38, 3.88, 3.85. The ^{13}C NMR data were not obtained due to the low solubility of the obtained polymer.

P1a/2e/3a. Yellow solid; yield <10% (Table 6, entry 10). M_w 4400; M_w/M_n 1.7 (GPC, polystyrene calibration). IR (film), ν (cm^{-1}): 2926, 2857, 1730, 1598, 1495, 1449. ^1H NMR (400 MHz, $CDCl_3$), δ (TMS, ppm): 7.11, 6.98, 3.75, 3.69, 3.68, 1.55, 1.25, 0.88, 0.71. The ^{13}C NMR data were not obtained due to the low solubility of the obtained polymer.

P1a/2f/3a. Red oil; yield <10% (Table 6, entry 11). M_w 4500; M_w/M_n 1.5 (GPC, polystyrene calibration). IR (film), ν (cm^{-1}): 2925, 2857, 1736, 1674, 1599, 1497, 1457. ^1H NMR (400 MHz, $CDCl_3$), δ (TMS, ppm): 7.11, 6.98, 4.05, 4.02, 3.81, 3.72, 3.61, 3.60, 1.56, 1.25, 0.85. The ^{13}C NMR data were not obtained due to the low solubility of the obtained polymer.

P1a/2a/3b. Yellow solid; yield 68.9% (Table 6, entry 12). M_w 5300; M_w/M_n 1.9 (GPC, polystyrene calibration). IR (film), ν (cm^{-1}): 2954, 2390, 1731, 1603, 1504, 1441. ^1H NMR (400 MHz, $CDCl_3$), δ (TMS, ppm): 7.12, 6.98, 5.01, 3.79, 3.52, 3.49, 3.03, 2.93. ^{13}C NMR (100 MHz, $CDCl_3$), δ (TMS, ppm): 178.36, 142.68, 135.78, 131.46, 128.25, 125.52, 91.92, 88.45, 83.47, 67.97, 53.70, 49.01, 34.22.

Model Reaction. Model compound **4** was prepared by coupling reaction of **9**, L-phenylalanine methyl ester hydrochloride (**2a**), and formaldehyde (**3a**). The experimental procedure was similar to that for the preparation of P**1a**/**2a**/**3a** but in the absence of organic solvent. Light yellow solid; yield 27.3%. IR (film), ν (cm^{-1}): 3066, 2954, 2862, 2355, 2249, 1953, 1887, 1809, 1731, 1596, 1496, 1445. ^1H NMR (400 MHz, $CDCl_3$), δ (TMS, ppm): 7.16, 7.14, 7.12, 7.10, 7.09, 7.02, 7.01, 7.00, 3.88, 3.87, 3.49, 3.11. ^{13}C NMR (100 MHz, $CDCl_3$), δ (TMS, ppm): 172.23, 143.85, 143.41, 140.24, 137.55, 131.23, 129.21, 128.79, 127.78, 126.63, 126.57, 120.78, 85.29, 84.86, 51.57, 41.11, 36.37. HRMS (MALDI-TOF): m/z 915.3992 (M^+, calcd 915.4076).

Photopatterning. The photo-cross-linking reaction of the polymer films was conducted in air at room temperature using 365 nm light obtained from a Spectroline ENF-280C/F UV lamp. The procedures were similar to those described in our previous publication.[12e]

RESULTS AND DISCUSSION

Table 1. Solvent Effect on the Polymerization of 1a, 2a, and 3a[a]

entry	solvent	yield (%)	M_w[b]	M_w/M_n[b]
1	toluene	73.9	24800	2.2
2	DMF	62.0	9400	1.7
3	dioxane	67.2	2200	1.3
4	methanol	12.7	1200	1.5
5	ethanol	50.2	1200	1.6
6	THF	~100	gel	

[a] Polymerization at 100 °C under nitrogen for 5 h in the presence of CuCl. [**1a**] = [**2a**] = 1 M, [**3a**] = 3 M, [Cu] = 0.5 [**1a**]. Abbreviation: DMF = dimethylformamide, THF = tetrahydrofuran. [b] Determined by GPC in THF on the basis of a polystyrene calibration.

Table 2. Temperature Effect on the Polymerization of 1a, 2a, and 3a[a]

entry	temp (°C)	yield (%)	M_w[b]	M_w/M_n[b]
1	80	67.6	19900	2.0
2[c]	100	73.9	24800	2.2
3	120	24.2	3800	2.4

[a] Polymerization in toluene under nitrogen for 5 h in the presence of CuCl. [**1a**] = [**2a**] = 1 M, [**3a**] = 3 M, [Cu] = 0.5 [**1a**]. [b] Determined by GPC in THF on the basis of a polystyrene calibration. [c] Data taken from Table 1, entry 3.

Table 3. Concentration Effect on the Polymerization of 1a, 2a, and 3a[a]

entry	[1a] (M)	yield (%)	M_w[b]	M_w/M_n[b]
1	0.5	40.9	9600	2.2
2	1.0	73.9	24800	2.2
3	1.5	89.0	43800	3.0

[a] Polymerization at 100 °C in toluene under nitrogen for 5 h in the presence of CuCl. [**1a**]:[**2a**]:[**3a**]:[Cu] = 1:1:3:0.5. [b] Determined by GPC in THF on the basis of a polystyrene calibration. [c] Data taken from Table 1, entry 3.

Monomer Preparation. In order to develop the one-pot A^3-coupling reaction of alkyne, primary amine, and aldehyde into a versatile methodology for the construction of functional polymers, we designed and prepared a group of diyne monomers with different molecular structures (Scheme 2). While monomers **1a**, **1c**, **1d**, and **1e** were synthesized according to the literature methods,[12] compound **1b** was prepared by the

Table 4. Effects of Different Catalysts and Their Loading on the Polymerization of 1a, 2a, and 3a[a]

entry	catalyst	loading (%)	yield (%)	M_w[b]	M_w/M_n[b]
1	CuCl	50	73.9	24800	2.2
2	CuI	50	10.0	2800	1.2
3	$Cu(OAc)_2$	50	29.7	3000	1.3
4	CuCl	30	52.5	4000	1.2

[a] Polymerization at 100 °C in toluene under nitrogen for 5 h. [**1a**] = [**2a**] = 1 M, [**3a**] = 3 M. [b] Determined by GPC in THF on the basis of a polystyrene calibration. [c] Data taken from Table 1, entry 3.

Table 5. Time Course on the Polymerization of 1a, 2a, and 3a[a]

entry	time (h)	M_w[b]	M_w/M_n[b]
1	1	26800	1.7
2	2	26900	1.7
3	5	24800	2.2

[a] Polymerization at 100 °C in toluene under nitrogen in the presence of CuCl. [**1a**] = [**2a**] = 1 M, [**3a**] = 3 M, [Cu] = 0.5 [**1a**]. [b] Determined by GPC in THF on the basis of a polystyrene calibration.

Table 6. Polymerization Results of Different Monomers[a]

entry	monomer	yield (%)	M_w[b]	M_w/M_n[b]	DP[c]	S[d]
1	**1a**/**2a**/**3a**	82.0	29200	4.6	10.9	√
2	**1b**/**2a**/**3a**	59.2	16700	2.0	14.3	√
3	**1c**/**2a**/**3a**	50.7	15700	2.1	10.0	√
4	**1d**/**2a**/**3a**	52.7	2700	2.0	1.7	Δ
5	**1e**/**2a**/**3a**	14.6	2100	1.8	2.5	√
6	**1f**/**2a**/**3a**	12.7	1500	1.6	3.0	Δ
7	**1a**/**2b**/**3a**	56.7	11800	2.2	9.2	√
8	**1a**/**2c**/**3a**	57.1				×
9	**1a**/**2d**/**3a**	7.2	4100	1.7	4.4	√
10	**1a**/**2e**/**3a**	<10	4400	1.7	4.7	√
11	**1a**/**2f**/**3a**	<10	4500	1.5	5.3	√
12	**1a**/**2a**/**3b**	68.9	5300	1.9	3.8	√

[a] Polymerization at 100 °C in toluene for 2 h under nitrogen in the presence of CuCl. [**1a**] = [**2a**] = 1 M, [**3a**] = 3 M, [Cu] = 0.5 [**1a**]. [b] Determined by GPC in THF on the basis of a polystyrene calibration. [c] Degree of polymerization. [d] Solubility (S) tested in common organic solvents, such as dichloromethane, chloroform, and tetrahydrofuran: √ = completely soluble, Δ = partially soluble, × = insoluble.

synthetic route shown in Scheme 3. Monomers **1f**, **2a**–**f**, and **3a**–**b** were commercially available and used without purification. All the synthesized monomers were characterized by standard spectroscopic techniques with satisfactory analysis data (see data given in the Experimental Section).

Polymerization Reaction. With the aim of optimizing the reaction conditions, we first studied the effect of different solvents on the polymerization using **1a**, **2a**, and **3a** as model monomers. The polymerization was carried out at 100 °C under nitrogen for 5 h in the presence of copper(I) chloride. As shown in Table 1, the solvents exerts a strong influence on the polymerization. Among all the tested organic solvents, toluene is proved to be the most suitable one, giving a polymer with the highest molecular weight (M_w = 24 800) in the highest yield of 73.9% (Table 1, entry 3). It is noteworthy that **3a** is utilized in aqueous solution, revealing that the polymerization is somewhat moisture-insensitive. Satisfactory results are also obtained in dimethylformamide, but PDAs with lower molecular weights are generated in dioxane, methanol, and ethanol despite that the yield, in some occasions, exceeds 50%. Gelation was observed when the polymerization was carried out in THF, probably due to the formation of polymers with extremely high molecular weights.

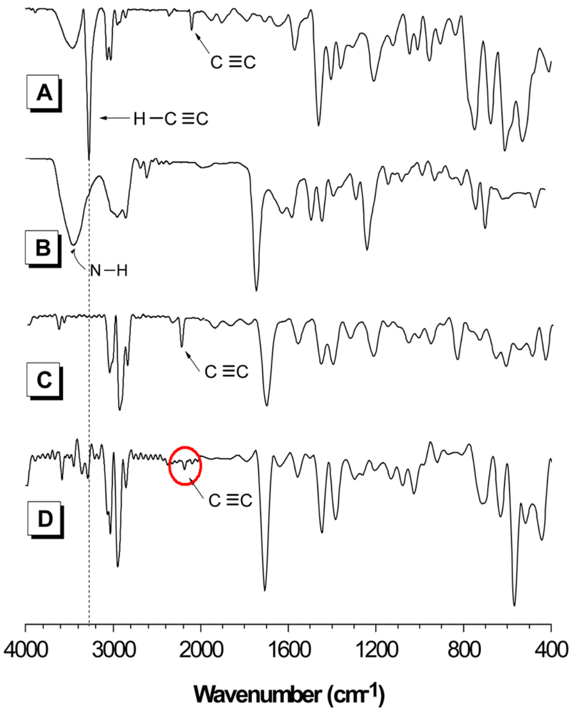

Figure 1. IR spectra of (A) **1a**, (B) **2a**, (C) model compound **4**, and (D) polymer P**1a**/**2a**/**3a**.

We then investigated the temperature effect on the polymerization. At 80 °C, a polymer with a high molecular weight (M_w = 19 900) was generated in ~68% yield (Table 2, entry 1). The yield and molecular weight were further enhanced when the temperature was raised to 100 °C. Further increment of the polymerization temperature to 120 °C led to a poorer result, probably because of the undesired side-reactions triggered by the high temperature.

Table 3 shows the effect of diyne concentration on the polymerization. Generally, polymerization at a higher monomer concentration will give a better result due to the more efficient intermolecular collision between molecules. Indeed, when the diyne concentration was gradually increased from 0.5 to 1.0 M

Scheme 4. Synthesis of Model Compound 4

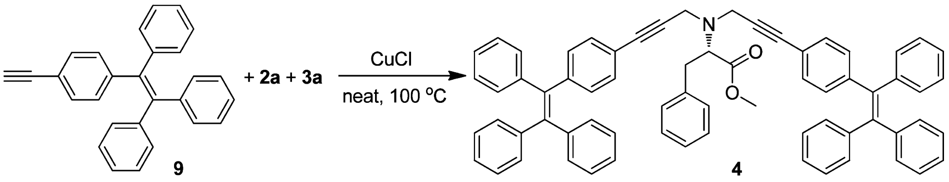

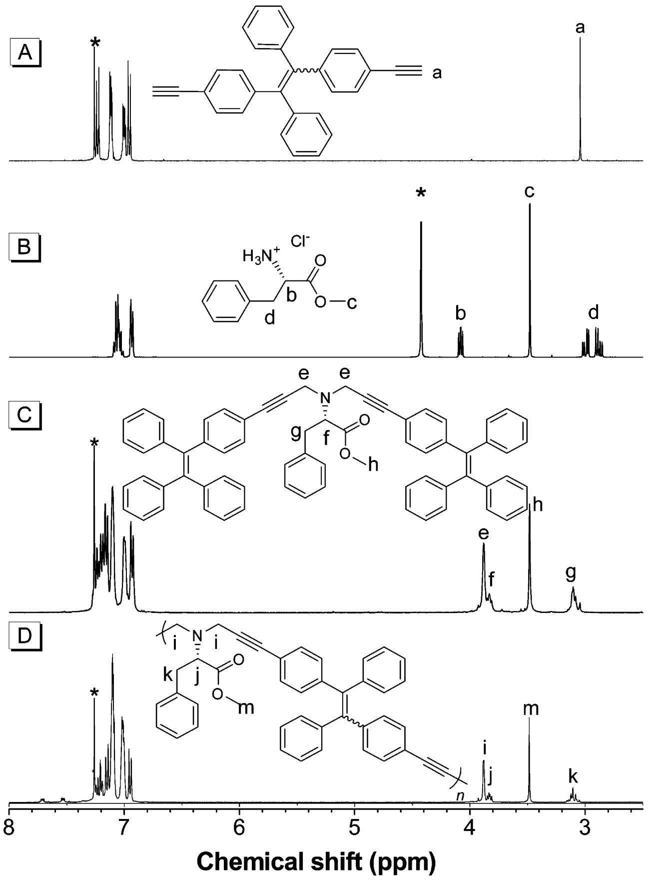

Figure 2. ^{1}H NMR spectra of (A) **1a**, (B) **2a**, (C) model compound **4**, and (D) polymer P**1a**/**2a**/**3a** in (A, C, and D) $CDCl_3$ and (B) D_2O. The solvent peaks are marked with asterisks.

and finally 1.5 M, the yield and molecular weight of the obtained polymer were enhanced by more than 2- and 4-fold, respectively. Since most of the monomers were not commercially available, a diyne concentration of 1 M was utilized for the subsequent investigation.

An array of copper salts is then examined for their efficiency to catalyze the A^3-coupling polymerization. It turns out that copper(I) chloride is the most efficient catalyst for the polymerization (Table 4, entry 1). On the contrary, neither copper(I) iodide nor copper acetate can initiate the polycoupling reaction. Previous study shows that the copper(I) cation takes an important role in the mechanism of the A^3-coupling reaction.[13] The higher ionic character of CuCl than CuI and $Cu(OAc)_2$ should be, in most cases, responsible for its higher catalytic efficiency. Both the molecular weight and yield of the resultant polymer were decreased significantly when a reduced catalyst loading was used for the polymerization (Table 4, entry 4).

We then followed the time course on the polymerization by GPC analysis of a small amount of reaction mixture extracted at a particular time using a pipet. As shown in Table 5, stirring a toluene solution of **1a**, **2a**, and **3a** for 1 h already gives a polymer with a reasonably high molecular weight. Prolonging the reaction time to 2 h affects little the molecular weight but improves the yield to a large extent. No further enhancement in the polymerization result was observed when the reaction time was lengthened to 5 h.

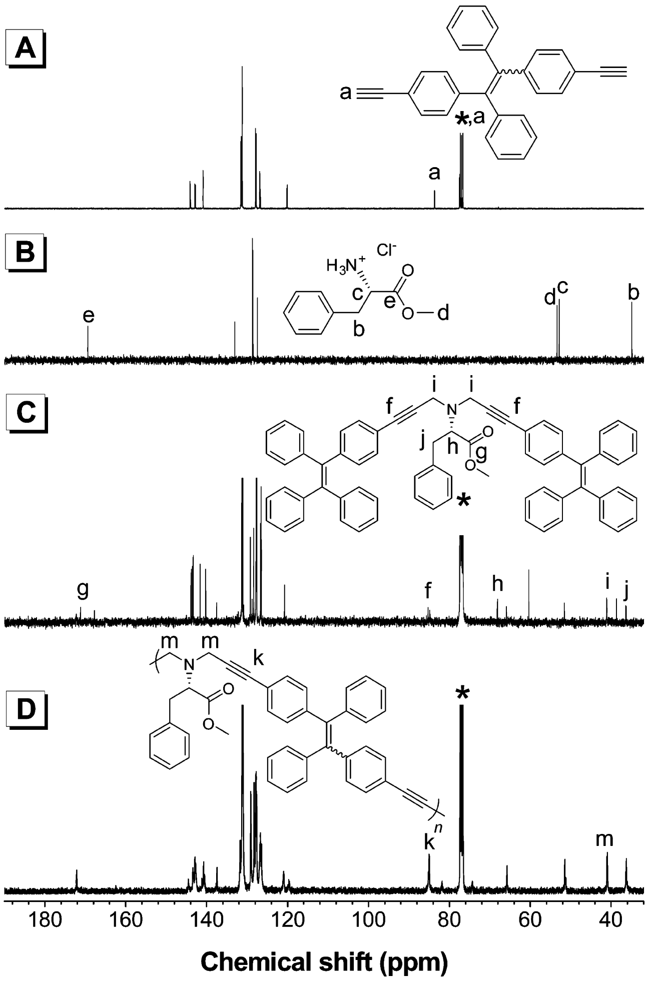

Figure 3. ^{13}C NMR spectra of (A) **1a**, (B) **2a**, (C) **4**, and (D) P**1a**/**2a**/**3a** in (A, C, and D) $CDCl_3$ and (B) D_2O. The solvent peaks are marked with asterisks.

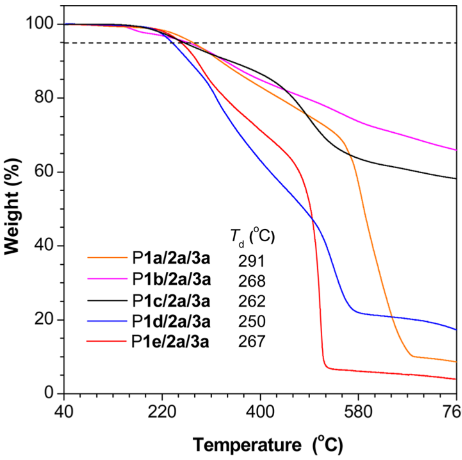

Figure 4. TGA thermograms of P**1a**–**e**/**2a**/**3a** recorded under nitrogen at a heating rate of 10 °C/min.

Table 6 shows the polymerization results of various combinations of diynes, primary amines, and aldehydes. Most of the polymerizations proceed smoothly, generating soluble PDAs with moderate to high molecular weights (M_w = 9600–43 800) in moderate to high yields (50.7–89.0%). PDAs generated from sterically more crowded diynes (**1b** and **1d**)

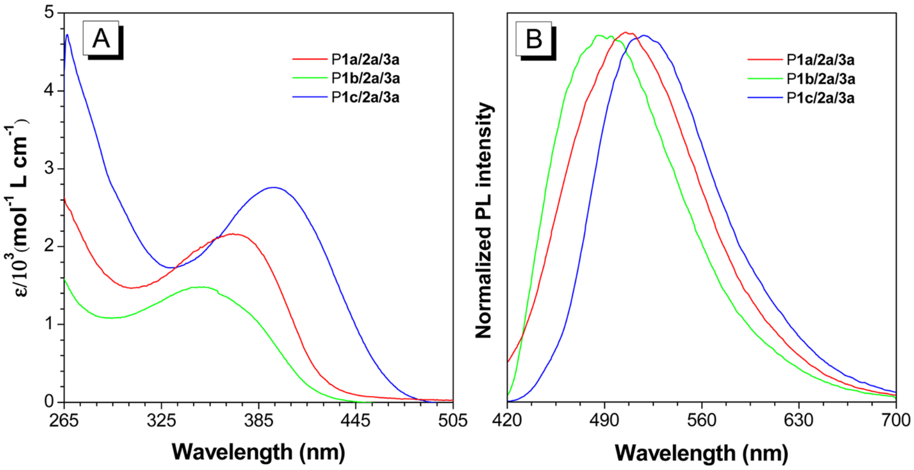

Figure 5. (A) UV and (B) PL spectra of P**1a**−**c**/**2**/**3** in THF solutions. Solution concentration: 10 μM; excitation wavelength (nm): 371 (P**1a**/**2a**/**3a**), 350 (P**1b**/**2a**/**3a**), 395 (P**1c**/**2a**/**3a**).

Table 7. Optical Properties of the PADs

polymer	λ_{abs}^{a} (nm)	λ_{em}^{a} (nm)	$\Phi_{F,S}$^{b} (%)
P**1a**/**2a**/**3a**	371	505	1.8
P**1b**/**2a**/**3a**	350	491	2.6
P**1c**/**2a**/**3a**	395	527	1.9

[a] In dilute THF solution (10 μM). Abbreviation: λ_{abs} = absorption maximum, λ_{em} = emission maximum. [b] $\Phi_{F,S}$ = fluorescence quantum yields of the polymer thin films measured by an integrated sphere.

normally possess lower molecular weights than those prepared from the less bulky ones (Table 6, entries 1−4). On the other hand, diynes (**1e** and **1f**) seem to show a lower polymerizability than their counterparts with aromatic rings (**1a**−**1c**). Regarding the primary amines, those with carboxylate group next to the amino functionality and phenyl ring (**1a**−**1c**) tend to be good monomers for the polymerization, probably due to the involved electronic effect.

Synthesis of Model Compound. To confirm the occurrence of the A^3-polycoupling reaction and to assist structural characterization of the obtained polymers, a model reaction was carried out according to the synthetic route shown in Scheme 4. The coupling reaction of TPE-containing monoyne **9**, **2a**, and **3a** was carried out under a semineat condition without organic solvent at 100 °C for 2 h. After purification by column chromatography, compound **4** was characterized by standard spectroscopic techniques.

Structural Characterization. All the polymers were characterized by IR and NMR spectroscopies. An example of the IR spectra of **1a**, **2a**, **4**, and P**1a**/**2a**/**3a** is given in Figure 1. While the absorption bands at 2106 and 3024 cm^{-1} in the spectrum of **1a** are stemmed from its ≡C−H and C≡C stretching vibrations, that at 3276 cm^{-1} in **2a** is associated with the absorption of its amino functionality. Both these bands, however are not observed in the spectrum of P**1a**/**2a**/**3a**. On the other hand, the spectrum of the polymer shows C═O and C≡C stretching absorption bands of **4** at 1746 and 2247 cm^{-1}, revealing the occurrence of the polymerization.

Figure 2 depicts the ^{1}H NMR spectra of P**1a**/**2a**/**3a**, its monomers (**1a** and **2a**), and model compound **4**. The acetylene proton of **1a** resonates at δ 3.04, which disappears in the spectrum of P**1a**/**2a**/**3a**. This suggests the complete consumption of the triple bonds of **1a** by the polymerization. Instead, a new peak corresponding to the resonance of the

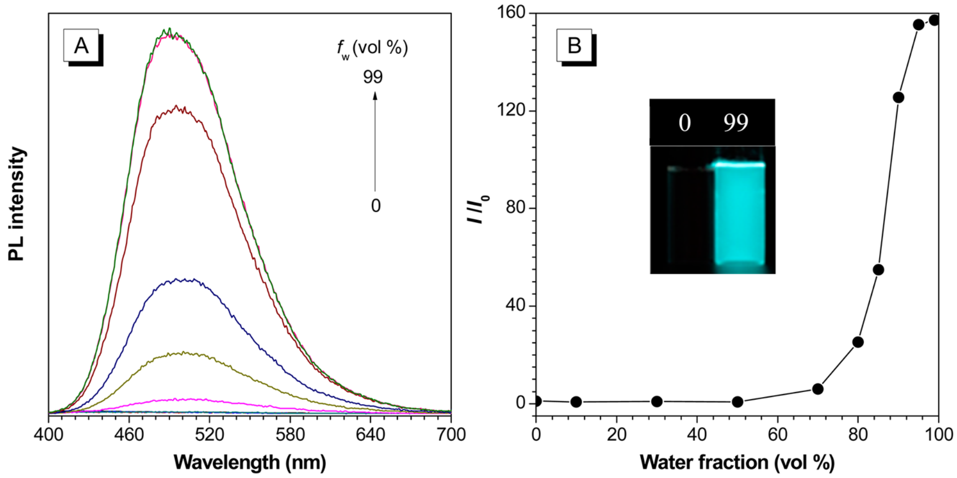

Figure 6. (A) PL spectra of **4** in THF and THF/H$_2$O mixtures with different water fractions (f_w). Concentration: 10 μM; excitation wavelength: 326 nm. Inset in (B): fluorescent photos of THF/water mixtures of **4** with different f_w taken under 365 nm UV irradiation. (B) Plot of relative PL intensity (I/I_0) versus the composition of the THF/H$_2$O mixture of **4**.

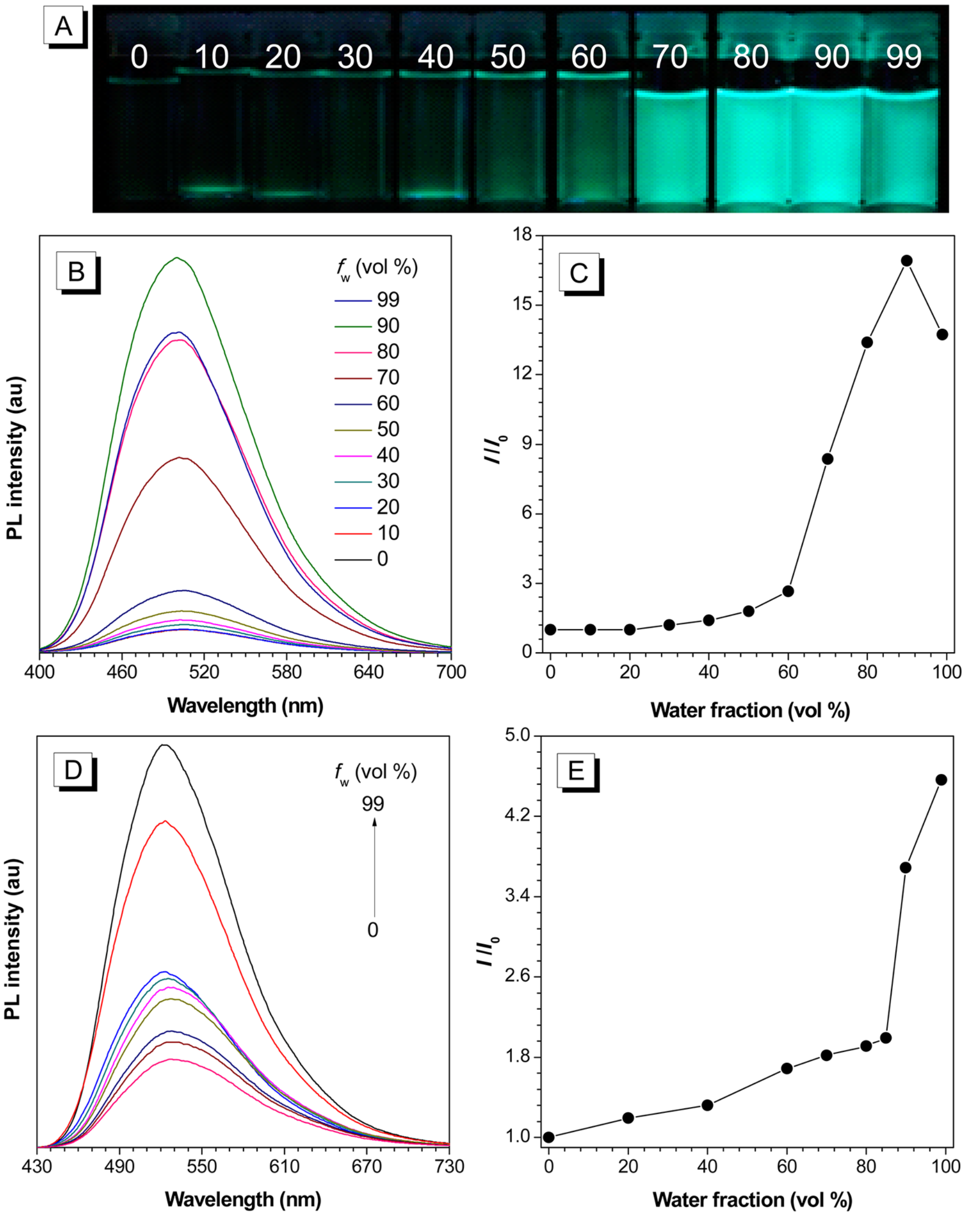

Figure 7. (A) Fluorescent photos of THF/H_2O mixtures of P**1a**/**2a**/**3a** with different water fraction (f_w) taken under 365 nm UV irradiation. PL spectra of (B) P**1a**/**2a**/**3a** and (D) P**1c**/**2a**/**3a** in THF and THF/H_2O mixtures with different (f_w). Concentration: 10 μM; excitation wavelength (nm): 371 (P**1a**/**2a**/**3a**) and 395 (P**1c**/**2a**/**3a**). Plot of relative PL intensity (I/I_0) versus the composition of the THF/H_2O mixtures of (C) P**1a**/**2a**/**3a** and (E) P**1c**/**2a**/**3a**.

methylene protons next to the triple bond functionality is emerged at δ 3.88 in P**1a**/**2a**/**3a**. Other absorption peaks can be readily assigned by comparing with the spectrum of **4**. This suggests that the polymeric product is indeed P**1a**/**2a**/**3a** with a molecular structure as shown in Scheme 2.

Similar information is provided by the ^{13}C NMR analysis. The internal acetylene carbon atom of **1a** absorbs at δ 83.65, which shifts to δ 84.96 after the polymerization (Figure 3). Meanwhile, a new peak associated with the resonance of the methylene carbons adjacent to the internal C≡C bond is emerged at δ 41.03 in the spectrum of P**1a**/**2a**/**3a**. These results are in well consistence with the results from IR and ^{1}H NMR measurements, further confirming the polymer structure.

Thermal Stability. As shown in Figure 4, all the polymers are thermally stable, losing merely 5% of their weight at high temperatures (T_d) ranging from 250 to 291 °C under nitrogen. P**1b**/**2a**/**3a** and P**1c**/**2a**/**3a** retain 60–70% of their weight after being heated to 800 °C. Thus, they can be applied as heat-resistance materials in many different fields.

Optical Properties. Figure 5A shows the UV spectra of **4** and PDAs in dilute THF solutions. They vary in shape and intensity due to their different structures and are peaked at 329–393 nm (Table 7). Among them, those containing silole moieties (P**1c**/**2a**–**b**/**3a**) display redder absorption maximum. From the UV analysis, it seems that P**1a**/**2a**/**3a** possesses a higher conjugation than P**1b**/**2a**/**3a** as the orbitals are distributed in a more linear and extended manner than in the former. When their dilute THF solutions are photoexcited, the PDAs emit green light at 505–541 nm (Figure 5B).

Emission quenching in the solid or aggregated state is often an obstacle to the practical applications of chromophoric polymers. The strong interactions between polymer chains in

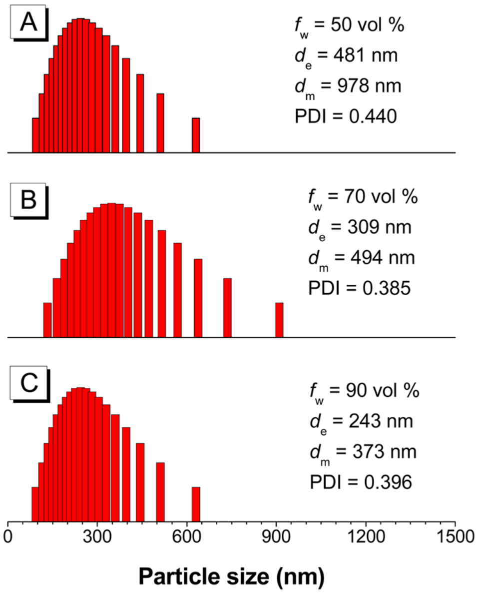

Figure 8. Particle size distributions of aggregates of **P1c/2a/3a** suspended in THF/water mixtures (10 μM) with water fractions (f_w) of (A) 50, (B) 70, and (C) 90 vol %. Abbreviation: d_e = effective diameter, d_m = mean diameter, PDI = polydispersity.

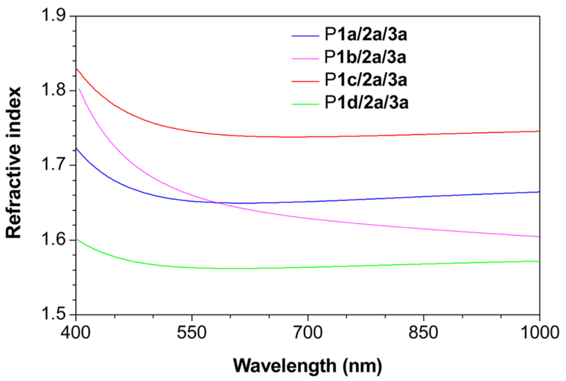

Figure 9. Wavelength dependence of refraction index of thin films of **P1a–d/2a/3a**.

Table 8. Refractive Indices and Chromatic Dispersions of P1/2a/3a[a]

polymer	$n_{632.8}$	ν_D	D
P1a/2a/3a	1.6498	46.7626	0.0214
P1b/2a/3a	1.6555	12.4045	0.0806
P1c/2a/3a	1.7389	31.4025	0.0318
P1d/2a/3a	1.5623	85.1818	0.0117

[a] Abbreviation: n = refractive index, ν_D = Abbé number = $(n_D - 1)/(n_F - n_C)$, where n_D, n_F, and n_C are the RI values at wavelengths of Fraunhofer D, F, and C spectral lines of 589.2, 486.1, and 656.3 nm, respectively; $D = 1/\nu_D$.

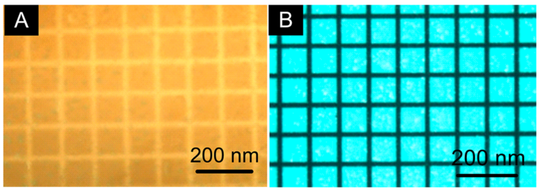

Figure 10. Negative photopatterns generated by photolithography of a film of **P1a/2a/3a** through a copper mask taken under (A) normal light illumination and (B) UV irradiation. Excitation wavelength: 330–385 nm.

the aggregated state usually lead to the formation of detrimental species such as excimers and exciplexes, which generally decay via nonradiative pathways. This effect is well-known as aggregation-caused quenching (ACQ).[15] Recently our group has observed a phenomenon the aggregation-induced emission (AIE) that is the exact opposite of the ACQ effect. We discovered that some propeller-shaped molecules such as TPE and hexaphenylsilole are nonemissive in solutions but are induced to emit intensely upon aggregate formation. We proposed the restriction of intramolecular motions as the main cause of the AIE effect. In the solution state, the periphery phenyl rings undergo free motions, which consumes the energy of the excited state through nonradiative relaxation channel. In solid or aggregated state, these motions are restricted, thus enabling the luminogens to relax radiatively. As a result, the polymers constructed from TPE- or silole-containing monomers are anticipated to show the AIE phenomenon as well.

As depicted in Figure 6A, the dilute THF solution (10 μM) of the model compound **4** emits almost no light upon photoexcitation. The PL intensity, however, rises gradually when an increasing amount of water is added to the THF solution. At 99% water content, the PL intensity is 160-fold higher than that in pure THF solution. Since **4** is insoluble in water, its molecules must form aggregates in aqueous solutions with high water contents. Clearly, **4** is AIE-active. Polymer **P1a/2a/3a** is also proved to be AIE-active, as suggested by the fluorescent photos shown in Figure 7A. The emission from the THF solution is still weak when up to 50% of water is added to the solution. Afterward, the PL becomes stronger progressively. Similar result was also obtained from the PL analysis (Figure 7B). The slight drop in the fluorescence intensity at 99% water fraction (Figure 7C) is probably due to the formation of extensive aggregates, which has lowered the "effective" solute concentration and hence the light emission. **P1c/2a/3a** shows similar emission behaviors, but it emits at longer wavelength region due to its higher conjugation (Figure 7D,E).

It is noteworthy that all the aqueous mixtures of **P1a/2a/3a** and **P1c/2a/3a** are visually transparent, suggesting that the polymer aggregates are of nanodimension. Indeed, the particle size analysis shows that the existence of particles in THF/H_2O mixtures of **P1c/2a/3a** with effective diameters ranging from 481 to 243 nm (Figure 8). When the water fraction was progressively increased from 50% to 70% and then to 90%, the particle size was decreased accordingly. This tendency is reasonable: at low water fraction, the polymer chains aggregate partially, and the dissolved chains slowly cluster to form "larger" particles. On the other hand, a large proportion of the polymer chains may aggregate quickly in the presence of a large amount of water, which finally gives nanoparticles with "smaller" effective diameters. The fluorescence quantum yields of thin films of **P1a–c/2a/3a** measured by an integrated sphere are within 1.8–2.6% (Table 7). Although these values are much lower than that (33.7%) of model compound **4**, probably due to the partial emission quenching by the defects in the polymers, the PDAs can be fabricated into thin solid films by a simple spin-coating process, which makes them suitable for the manufacture of large-area flat-panel devices.

Light Refraction. Advanced photonic devices are often composed of working units with high contrast of refractive

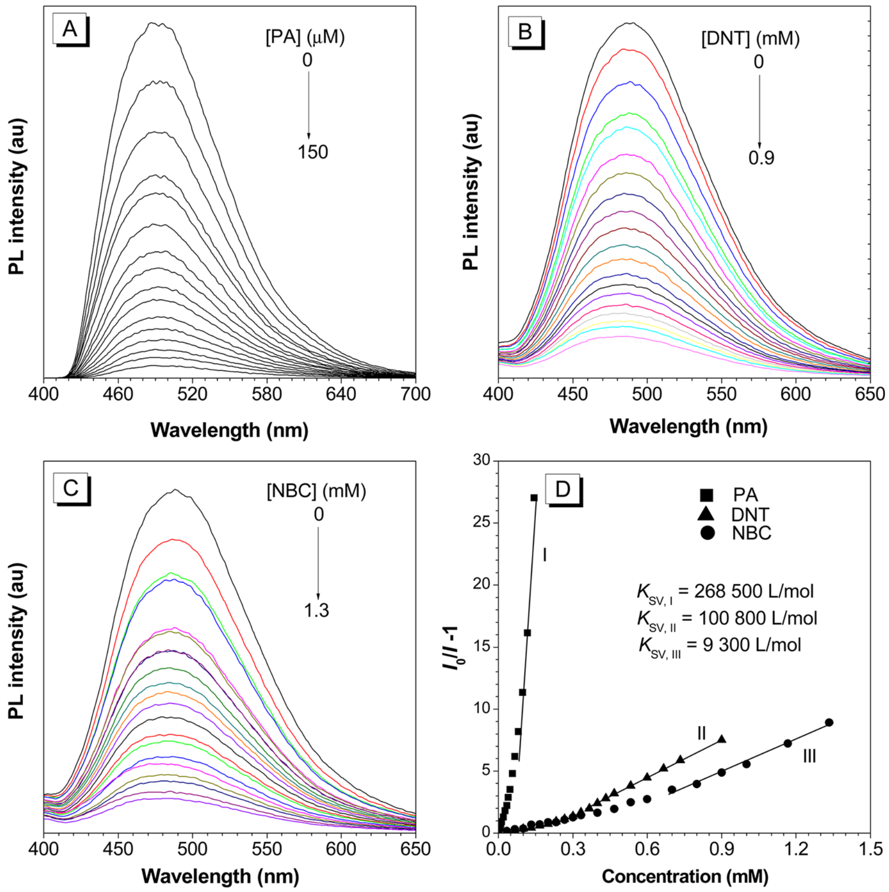

Figure 11. PL spectra of P**1b**/**2a**/**3a** in THF/H_2O mixture (1:9 v/v) containing different amounts of (A) picric acid (PA), (B) 2,4-dinitrotoluene (DNT), and (C) 4-nitrobenzoyl chloride (NBC). (D) Stern–Volmer plots of relative intensity ($I_0/I - 1$) versus the explosive concentration. I_0 = PL intensity in the absence of explosives.

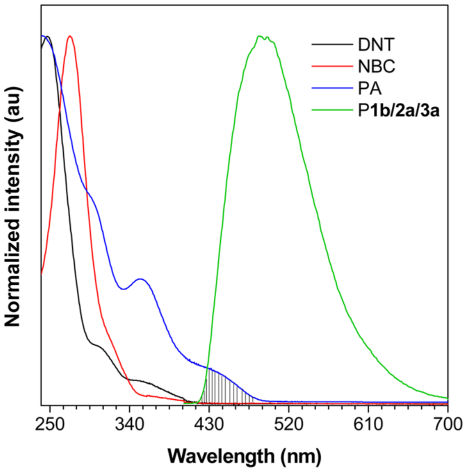

Figure 12. Normalized absorption spectra of DNT, NBC, and PA in THF and PL spectrum of P**1b**/**2a**/**3a** in THF/H_2O mixture (1:9 v/v).

index (RI). Polymers with high RI values can serve as promising candidates for a wide range of photonic applications, such as organic light-emitting diodes, lenses, waveguides, and image sensors.[16] Theoretically, polymers with highly polarized aromatic rings, heteroatoms, and acetylene units are liable to exhibit high RI values. As illustrated in Figure 9, P**1a**–**d**/**2a**/**3a** show RI of 1.8322–1.7458, 1.7787–1.6297, 1.7247–1.6645, and 1.6026–1.5719, respectively, in a wide wavelength region of 400–1000 nm, whose values are higher than those of commercial polymers,[17] such as polystyrene (n = 1.602–1.589) and polycarbonate (n = 1.593–1.576). Apparently, the high refractivity of the polymers bestows them with potential applications as photonic devices.

Chromatic Dispersion. The chromatic dispersion (D) is concerned with the wavelength dependence of the refractive index of a material. Large D value leads to undesired effect such as degradation of images resolution and limit. Thus, polymers with low chromatic dispersions are promising for applications as optical materials. The Abbé number (ν_D) is adopted to measure the variation or dispersion of a material and is defined as $(n_D - 1)/(n_F - n_C)$, where n_D, n_F, and n_C are the RI values at wavelengths of Fraunhofer D, F, and C spectral lines of 589.2, 486.1, and 656.3 nm, respectively.[18] The D value is the reciprocal of ν_D. As shown in Table 8, the ν_D and the corresponding D values of the polymers fall in the scale of 12.4–85.2 and 0.0117–0.0806. Evidently, most of our polymers have high Abbé numbers and hence low optical dispersions. This enables them to find an array of photonic applications such as coating materials and high-performance CMOS image sensors.[16]

Photopatterning. UV irradiation is a convenient and flexible source for the fabrication of luminescent patterns. Taking its advantages of good film-forming ability and strong emission in the solid state, UV irradiation of a spin-coated film of P**1a**/**2a**/**3a** on a silicon wafer through a copper mask can generate a well-resolved fluorescent pattern (Figure 10). The exposed parts (lines) of the films are cross-linked and are photobleached. Thus, they appear dark under UV illumination. The unexposed squares, on the other hand, emit brightly in the presence of UV light. The distinct pattern with sharp edges has proved the high efficiency of the technique for the construction of photonic and electronic devices and biological sensing and probing systems such as LCD, OLED, and medicinal diagnostic biochip.[19]

Explosive Detection. The AIE property of P**1b**/**2a**/**3a** inspires us to explore its potential applications as a chemosensor for explosive because of the involved antiterrorism implication. 2,4,6-Trinitrophenol (picric acid, PA), 2,4-dinitrotoluene (DNT), and 4-nitrobenzoyl chloride (NBC) are used as model compounds for their commercial availability and distinction in high nitro group content. The nanoaggregates in 90% aqueous mixture with a concentration of 10 μM are utilized as probes. As shown in Figure 11, the PL of the nanoaggregates is weakened gradually when an increasing amount of explosives is added to the aqueous solution. At PA, DNT, and NBC concentration of 150 μM, 0.9 mM, and 1.3 mM, respectively, the emission is completed quenched. The detection limit is found to be 1 μM. The Stern−Volmer plots of relative PL intensity ($I_0/I - 1$) versus the explosive concentration all give curves bending upward, indicating a more sensitive and efficient quenching process with an increasing quencher concentration (Figure 11D).

There is a noticeable disparity in the quenching efficiency toward different explosives. As deduced in Figure 11D, the quenching constants of PA, DNT, and NBC determined from the linear region of the Stern−Volmer plots are 268 500, 100 800, and 9300 L/mol, respectively. To explain such selectivity, the absorption of PA, DNT, and NBC was measured and compared with the PL spectrum of P**1b**/**2a**/**3a** (Figure 12). In the wavelength region of 415−500 nm, the UV spectrum of PA and the PL spectrum of the polymer are overlapped. This should lead to energy transfer from the excited state of P**1b**/**2a**/**3a** to the ground state of PA and hence nonradiative relaxation.[20] On the contrary, DNT and NBC do not absorb at wavelengths where the polymer emits, thus accounting for their weak quenching effect. On the other hand, the Lewis acid−base interaction between the electron-efficient polymer chains and the electron-deficient quencher molecules may also account for the quenching phenomenon. Considering its highest nitro group content, PA is supposed to exert the strongest electron-withdrawing effect among the three explosives and hence shows higher quenching efficiency. Generally, aggregation of fluorescent conjugated polymers causes the ACQ problem and thus reduces their sensing performance. However, aggregation is beneficial to the PL of P**1b**/**2a**/**3a**. Moreover, its aggregates have many cavities to bind with quencher molecules and provide additional interchain diffusion pathways for excitons to migrate. These collective effects thus make the PL annihilation a highly efficient process.

■ CONCLUSIONS

In this work, we succeeded in developing a new synthetic route to functional macromolecules from alkynes, primary amines, and aldehydes. This one-pot A^3-coupling polymerization is catalyzed by a cheap catalyst of copper(I) chloride and is tolerant to moisture. The polymerization reaction can be completed in a short period of time, generating high molecular weight PDAs in high yields. The obtained polymers are soluble and thermally stable and can be fabricated into good films. They show high refractive indices with low small chromatic dispersions. Some PDAs are AIE-active and exhibit strong emissions in the solid or aggregated state. They are photosensitive and can generate negative photoresist patterns upon UV irradiation. They can function as fluorescent chemosensors for sensitive detection of explosives. Since the present polymers contain abundant triple bonds in their backbones, they are promising candidates for organometallic materials and magnetic ceramics. Additionally, the propargylamine substructure of the polymers enables them to be further functionalized by reactions such as "click" chemistry. As the amino acid segments are chiral and capable of forming hydrogen bond, they may impart the polymers with novel chiroptical and self-assembly properties. All these possibilities are currently under investigation in our laboratory.

■ AUTHOR INFORMATION

Corresponding Authors

*E-mail chjacky@ust.hk; Ph +852-2358-7375(7242); Fax +852-2358-1594 (J.W.Y.L.).
*E-mail tangbenz@ust.hk; Ph +852-2358-7375(7242); Fax +852-2358-1594 (B.Z.T.).

Notes

The authors declare no competing financial interest.

■ ACKNOWLEDGMENTS

This work was partially supported by the National Basic Research Program of China (973 Program; 2013CB834701), the Research Grants Council of Hong Kong (604913, 604711, 6602212, and N_HKUST620/11), the Nissan Chemical Industries, Ltd., the Innovation and Technology Commission (ITCPD117-9), and the University Grants Committee of Hong Kong (AoE/P-03/08). B.Z.T. thanks the support of the Guangdong Innovative Research Team Program (201101C0105067115).

■ REFERENCES

(1) (a) Ochiai, B.; Ogihara, T.; Mashiko, M.; Endo, T. *J. Am. Chem. Soc.* **2009**, *131*, 1636−1637. (b) Wang, Y.-Z.; Deng, X.-X; Li, L.; Li, Z.-L.; Du, F.-S.; Li, Z.-C. *Polym. Chem.* **2013**, *4*, 444−448. (c) Li, L.; Kan, X.-W.; Deng, X.-X.; Song, C.-C.; Du, F.-S.; Li, Z.-C. *J. Polym. Sci., Part A: Polym. Chem.* **2013**, *51*, 865−873.

(2) (a) Ugi, I.; Domling, A.; Werner, B. *J. Heterocycl. Chem.* **2000**, *37*, 647−658. (b) Weber, L.; Illgen, K.; Almstetter, M. *Synlett* **1999**, 366−374. (c) Armstrong, R. W.; Combs, A. P.; Tempest, P. A.; Brown, S. D.; Keating, T. A. *Acc. Chem. Res.* **1996**, *29*, 123−131.

(3) (a) Li, C. J.; Wei, C. *Chem. Commun.* **2002**, 268−269. (b) Li, C. J. *Acc. Chem. Res.* **2010**, *43*, 581−590. (c) Wei, C.; Li, Z.; Li, C. J. *Synlett* **2004**, *9*, 1472−1483.

(4) Sakai, N.; Uchida, N.; Konakahara, T. *Synlett* **2008**, *10*, 1515−1519.

(5) Li, P.; Wang, L.; Zhang, Y.; Wang, M. *Tetrahedron Lett.* **2008**, *49*, 6650−6654.

(6) Eshghi, H.; Zohuri, G. H.; Damavandi, S. *Eur. J. Med. Chem.* **2011**, *2*, 100−103.

(7) He, Y.; Lv, M. F.; Cai, C. *Dalton Trans.* **2012**, *41*, 12428−12433.

(8) Uhlig, N.; Li, C. J. *J. Org. Lett.* **2012**, *14*, 3000−3003.

(9) (a) Qin, A. J.; Lam, J. W. Y.; Tang, B. Z. *Chem. Soc. Rev.* **2010**, *39*, 2522−2544. (b) Liu, J.; Lam, J. W. Y.; Tang, B. Z. *Chem. Rev.* **2009**, *109*, 5799−5867. (c) Lam, J. W. Y.; Tang, B. Z. *Acc. Chem. Res.* **2005**, *38*, 745−754.

(10) Chan, C. Y. K.; Tseng, N. W.; Lam, J. W. Y.; Liu, J.; Kwok, R. T. K.; Tang, B. Z. *Macromolecules* **2013**, *46*, 3246−3256.

(11) (a) Manners, I. *Science* **2001**, *294*, 1664−1666. (b) Babudri, F.; Farinola, G. M.; Naso, F. *J. Mater. Chem.* **2004**, *14*, 11−34. (c) Chan, W. Y.; Berenbaum, A.; Clendenning, S. B.; Lough, A. J.; Manners, I.

Organometallics **2003**, *22*, 3796−3808. (d) Long, N. J.; Williams, C. K. *Angew. Chem., Int. Ed.* **2003**, *42*, 2586−2617. (e) Bunz, U. H. F. *J. Organomet. Chem.* **2003**, *683*, 269−287.

(12) (a) Hu, R. R.; Maldonado, J. L.; Rodriguez, M.; Deng, C.; Jim, C. K. W.; Lam, J. W. Y.; Yuen, M. M. F.; Tang, B. Z. *J. Mater. Chem.* **2012**, *22*, 232−240. (b) Hu, R. R.; Ye, R.; Lam, J. W. Y.; Li, M.; Leung, C. W. T.; Tang, B. Z. *Chem.—Asian J.* **2013**, *8*, 2436−2445. (c) Liu, J.; Zhong, Y.; Lam, J. W. Y.; Lu, P.; Hong, Y.; Yu, Y.; Yue, Y.; Faisal, M.; Sung, H. H. Y.; Williams, I. D.; Wong, L. S.; Tang, B. Z. *Macromolecules* **2010**, *43*, 4921−4936. (d) Hu, R.; Lam, J. W. Y.; Liu, J.; Sung, H. H. Y.; Williams, I. P.; Yue, Z.; Wong, L. S.; Yuen, M. M. F.; Tang, B. Z. *Polym. Chem.* **2012**, *3*, 1481−1489. (e) Hu, R.; Lam, J. W. Y.; Yu, Y.; Sung, H. H. Y.; Williams, I. D.; Yuen, M. M. F.; Tang, B. Z. *Polym. Chem.* **2013**, *4*, 95−105.

(13) Bariwal, J. B.; Ermolat'ev, D. S.; Eycken, V. E. V. *Chem.—Eur. J.* **2010**, *16*, 3281−3284.

(14) Birks, J. B. *Photophysics of Aromatic Molecules*; Wiley: London, 1970.

(15) (a) Hong, Y.; Lam, J. W. Y.; Tang, B. Z. *Chem. Soc. Rev.* **2011**, *40*, 5361−5388. (b) Hong, Y.; Lam, J. W. Y.; Tang, B. Z. *Chem. Commun.* **2009**, *29*, 4332−4353. (c) Luo, J. D.; Xie, Z. L.; Lam, J. W. Y.; Cheng, L.; Chen, H. Y.; Qiu, C. F.; Kwok, H. S.; Zhan, X. W.; Liu, Y. Q.; Zhu, D. B.; Tang, B. Z. *Chem. Commun.* **2001**, 1740−1741.

(16) Liu, J.; Ueda, M. *J. Mater. Chem.* **2009**, *19*, 8907−8919 and references therein.

(17) (a) Seferis, J. C. *Polymer Handbook*, 3rd ed.; Brandrup, J., Immergut, E. H., Eds.; Wiley: New York, 1989; pp VI/451−VI/461. (b) Mills, N. J. *Concise Encyclopedia of Polymer Science & Engineering*; Kroschwitz, J. I., Ed.; Wiley: New York, 1990; pp 683−687.

(18) Hecht, E. *Optics*, 4th ed.; Addison Wesley: San Francisco, CA, 2002.

(19) (a) Campbell, L.; Sharp, D. N.; Harrison, M. T.; Denning, R. G.; Turberfield, A. J. *Nature* **2000**, *404*, 53−56. (b) Kim, J. M. *Macromol. Rapid Commun.* **2007**, *28*, 1191−1212.

(20) Wang, J.; Mei, J.; Yuan, W.; Lu, P.; Qin, A.; Sun, J.; Ma, Y.; Tang, B. Z. *J. Mater. Chem.* **2011**, *21*, 4056−4059.